PAPER

A run-and-tumble particle around a spherical obstacle: the steady-state distribution far-from-equilibrium

Journal of Statistical Mechanics: Theory and Experiment
An IOP and SISSA journal

PAPER: Classical statistical mechanics, equilibrium and non-equilibrium

A run-and-tumble particle around a spherical obstacle: the steady-state distribution far-from-equilibrium

Thibaut Arnoulx de Pirey[1,*] **and Frédéric van Wijland**[2]

[1] Department of Physics, Technion-Israel Institute of Technology, Haifa 32000, Israel
[2] Laboratoire Matière et Systèmes Complexes, Université Paris Cité & CNRS (UMR 7057), 10 rue Alice Domon et Léonie Duquet, 75013 Paris, France
E-mail: t.depirey@campus.technion.ac.il

Received 1 March 2023
Accepted for publication 30 June 2023
Published 12 December 2023

Online at stacks.iop.org/JSTAT/2023/093202
https://doi.org/10.1088/1742-5468/ace42d

Abstract. We investigate the steady-state distribution function of a run-and-tumble particle (RTP) evolving around a repulsive hard spherical obstacle. We demonstrate that the well-documented activity-induced attraction translates into a delta-peak accumulation at the obstacle's surface accompanied by an algebraic divergence of the density profile close to the obstacle. We obtain the full form of the distribution function in the regime where the typical distance run by the particle between two consecutive tumbles is much larger than the obstacle's size. This finding provides an expression for the low-density pair distribution function of a fluid of highly persistent hard-core RTP. It also advances an expression for the steady-state probability distribution of highly ballistic active Brownian particles and active Ornstein–Uhlenbeck particles around hard spherical obstacles.

Keywords: statistical physics, stochastic dynamics, active matter, nonequilibrium processes

*Author to whom any correspondence should be addressed.

1742-5468/23/093202+31$33.00

Contents

1. Introduction

Such spectacular collective physical phenomena as collective alignment [1–3] or motility-induced phase separation [4–7], are trademarks of interacting active, self-propelled, particles. However, the individual behavior of an active particle interacting with an external potential exhibits equally puzzling features. For example, a steeper decay of density for sedimenting run-and-tumble particles (RTPs) under a constant gravity field [8], a depleted probability at the bottom of a harmonic well for RTPs [8–11] or active Brownian particles (ABPs), and more prominently perhaps, a tendency to be attracted to otherwise repulsive obstacles. For instance, this phenomenon has been explored in two-dimensional channels for RTPs [12] or ABPs [13], and more

J. Stat. Mech. (2023) 093202

generally for particles confined within walls [14, 15]. Physically more complicated systems have been considered, such as a needle-like particle interacting with a spherical obstacle [16] in the presence of a surrounding fluid, which adds hydrodynamic interactions to an already nontrivial problem. The understanding of the one-body problem is also instrumental in breaking down the mechanisms at work in many-body collective phenomena into elementary ones. In systems of particles interacting via pairwise forces considered in the dilute limit, one can, as in the virial approach familiar in equilibrium systems, focus on a single pair of particles. For this pair of particles, the associated reduced particle [17] evolves in an effective external potential. However, the statistics of the active self-propulsion force felt by the reduced particle need not—and will in general not—be identical to that exerted on each individual particle.

From a purely analytical standpoint, instances wherein the stationary distribution can be found exactly are scarce. A single RTP in one space dimension, in an arbitrary external potential or with a spatially varying tumble rate and speed [18–22], is a notable exception. This problem has also been solved on a one-dimensional lattice and in the continuum for an RTP between two hard walls [23, 24]. For the more realistic case of two hard-disk RTPs, an approximate treatment was recently put forward [25]. The objective of this work is to address the case of an RTP in contact with a hard spherical obstacle in space dimension d, with a particular emphasis on the highly ballistic limit where the persistence length ℓ_p of the RTP, that is the mean distance run by the free particles between two consecutive tumbles, is much larger than the obstacle size σ. In the highly ballistic regime, the particle thus almost never tumbles when near the obstacle. Incidentally, the highly ballistic limit turns out to be relevant for studying collective phenomena, such as the motility-induced phase separation [6]. This regime has also been examined for its connections with sheared granular systems [26, 27].

Our primary results are as follows. For all $\eta = \sigma/\ell_p$, the stationary distribution function is shown to exhibit a delta-peak accumulation at the surface of the obstacle and a density profile away from the obstacle (in the bulk of the system) that diverges at $r = \sigma$. The structure of this divergence is elucidated. We furthermore prove that the bulk distribution function in the position and self-propulsion space exhibits a delta-peak accumulation along typical trajectories of the stochastic dynamics, that we characterize. The steady-state distribution is then fully characterized in $d \geqslant 2$ as $\eta \to 0$. Corrections to this limiting behavior to the next order in η are also investigated, and we show that the amplitude of the delta-peak accumulation decreases as the persistence length is reduced. Finally, we demonstrate that in the highly ballistic limit $\eta \to 0$, far-field hydrodynamic interactions, as captured by the Oseen tensor, reduce the amplitude of the delta-peak accumulation.

We begin, in section 2, by introducing the particle model we consider and obtaining coupled equations for the bulk and surface contributions to the steady-state distribution. In section 3, we then express, in the steady state, the marginal density in the position space as the solution to an integral equation. This equation is solved near the obstacle in section 4 and in the highly ballistic regime in section 5. The effect of hydrodynamic interactions in the highly ballistic regime is investigated in section 6. Our conclusion, in section 7, discusses possible paths deserving of further exploration.

J. Stat. Mech. (2023) 093202

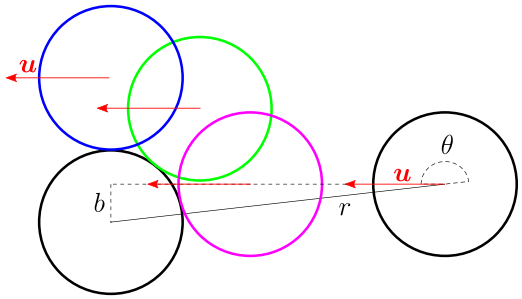

Figure 1. A collision of an active hard-sphere (black, rightmost) with diameter σ and impact parameter $b = r\sin\theta < \sigma$ (with $\cos\theta < 0$) onto a pinned (black, leftmost) one. The incoming particle with direction $\boldsymbol{u}$ hits the target sphere (at the magenta position) and then skids around, as in the green position. In the absence of tumbling, it eventually takes off at the blue position when its orientation $\boldsymbol{u}$ becomes tangent to the target sphere. In the highly ballistic limit, no tumble can occur over the typical skidding distances.

2. The steady-state distribution: bulk and surface contributions

In this section, we derive the equations satisfied by the steady-state probability distribution of an RTP evolving in the presence of a hard spherical obstacle in arbitrary space dimension $d > 1$. We prove that the latter splits into a bulk contribution and a surface contribution localized at the surface of the obstacle. We obtain coupled equations satisfied by these two contributions. The latter sections are devoted to reformulating these equations in terms of an integral equation for the density field which we solve in some limiting cases.

To achieve this result, we start with the equation of motion of an RTP evolving in a smooth spherically symmetric repulsive potential. The hard-sphere limit is carefully taken at a later stage. The position of the RTP evolves according to:

$$\frac{\mathrm{d}\boldsymbol{r}}{\mathrm{d}t} = v_0\boldsymbol{u}(t) - \boldsymbol{\nabla}V(\boldsymbol{r})\,, \tag{1}$$

where $\boldsymbol{u}(t)$ is a unit vector that is uniformly reoriented on the unit sphere with rate τ^{-1}. The potential is assumed to depend only on the distance $r = ||\boldsymbol{r}||$ so that $V(\boldsymbol{r}) = V(r)$. In figure 1 we depict the interactions between an incoming particle and a hard obstacle. Even though figure 1 shows an obstacle and a particle that have the same size, in practice, the results only depend on the exclusion radius of the hard-sphere potential, meaning the radius of the obstacle plus the radius of the particle. Figure 1 further illustrates the key difference with the physics of one-dimensional systems (or higher-dimensional ones in the presence of an extended flat wall). Here, the particle can leave the vicinity of the obstacle even in the absence of tumbling events. The stationary state distribution function $P(\boldsymbol{r},\boldsymbol{u})$ solves the master equation:

J. Stat. Mech. (2023) 093202

$$-v_0\boldsymbol{u}\cdot\boldsymbol{\nabla}_{\boldsymbol{r}}P(\boldsymbol{r},\boldsymbol{u})+\boldsymbol{\nabla}_{\boldsymbol{r}}\left(P(\boldsymbol{r},\boldsymbol{u})\boldsymbol{\nabla}_{\boldsymbol{r}}V(\boldsymbol{r})\right)+\frac{1}{\tau}\left(\int\frac{\mathrm{d}\boldsymbol{u}'}{\Omega_d}P(\boldsymbol{r},\boldsymbol{u}')-P(\boldsymbol{r},\boldsymbol{u})\right)=0\,. \tag{2}$$

We take advantage of the rotational symmetry to write $P(\boldsymbol{r},\boldsymbol{u})=P(r,w)$, where $w=\boldsymbol{r}\cdot\boldsymbol{u}/r=\cos\theta$ with θ the polar angle measured with respect to $\boldsymbol{u}$. Using these spherical coordinates, equation (2) becomes:

$$\begin{aligned}0=&-v_0\left(w\partial_rP(r,w)+\frac{1-w^2}{r}\partial_wP(r,w)\right)+\frac{1}{r^{d-1}}\partial_r\left(r^{d-1}P(r,w)\partial_rV(r)\right)\\&+\frac{1}{\tau}\left(\int_{-1}^{1}\frac{\mathrm{d}w'}{2W_{d-2}}\left(1-w'^2\right)^{\frac{d-3}{2}}P(r,w')-P(r,w)\right).\end{aligned} \tag{3}$$

Here, the normalization constant W_n is the nth Wallis integral:

$$W_n=\frac{1}{2}\int_{-1}^{1}\mathrm{d}w'\left(1-w'^2\right)^{\frac{n-1}{2}}\,. \tag{4}$$

The equations of motion written in terms of the variables r,w are discussed in appendix A. One of the ways of ultimately implementing a hard-sphere potential with exclusion diameter σ is to begin with a smoothly repulsive potential $V(r)$ of the form:

$$V(r)=V_0\,\mathrm{e}^{-\frac{r-\sigma}{\epsilon\sigma}}\,, \tag{5}$$

and to take the hard-sphere limit $\epsilon\to0^+$ by following the program explained in a previous study [28] and further detailed in what follows. For any fixed $r>\sigma$, we first define the bulk distribution function $f(r,w)$ as follows:

$$f(r,w)=\lim_{\epsilon\to0^+}P(r,w)\,. \tag{6}$$

It follows from equation (3) that

$$\begin{aligned}0=&-v_0\left(w\partial_rf(r,w)+\frac{1-w^2}{r}\partial_wf(r,w)\right)\\&+\frac{1}{\tau}\left(\int_{-1}^{1}\frac{\mathrm{d}w'}{2W_{d-2}}\left(1-w'^2\right)^{\frac{d-3}{2}}f(r,w')-f(r,w)\right),\end{aligned} \tag{7}$$

which expresses the flux balance between the free streaming of the particle for $r>\sigma$ under the action of the active self-propulsion and the random reorientation of the latter. We now turn to the behavior of the distribution function close to $r=\sigma$ and demonstrate that it develops a delta singularity when $\epsilon\to0^+$. From the equation of motion (1), we know that $\forall\epsilon>0$, $P(r,w)=0$ for $r\leqslant r^*$ with r^* defined by $V'(r^*)=-v_0$. Here, $r^*-\sigma=\epsilon\sigma\ln(\epsilon v_0/V_0)$ goes to 0 as $\epsilon\to0^+$. To identify the singularity, we define the surface distribution function as follows:

$$\Gamma(w)=\sigma^{-1}\lim_{r\to\sigma}\lim_{\epsilon\to0^+}\int_{r^*}^{r}\mathrm{d}r'P(r',w)\,. \tag{8}$$

J. Stat. Mech. (2023) 093202

We then multiply equation (3) by r^{d-1} and integrate it between r^* and some fixed $r > r^*$. After integration by part and using the boundary condition $P(r^*, w) = 0$, we obtain:

$$\begin{aligned} 0 = &-v_0 w r^{d-1} P(r,w) + v_0 (d-1) w \int_{r^*}^{r} \mathrm{d}r' r'^{d-2} P(r',w) \\ &+ r^{d-1} P(r,w) V'(r) - v_0 (1-w^2) \partial_w \int_{r^*}^{r} \mathrm{d}r' r'^{d-2} P(r',w) \\ &+ \frac{1}{\tau} \int_{r^*}^{r} \mathrm{d}r' r'^{d-1} \left(\int_{-1}^{1} \frac{\mathrm{d}w'}{2W_{d-2}} \left(1-w'^2\right)^{\frac{d-3}{2}} P(r',w') - P(r',w) \right) . \end{aligned} \tag{9}$$

At fixed r, we take the limit $\epsilon \to 0^+$ wherein the term proportional to $V'(r)$ vanishes. We then take the $r \to \sigma$ limit, yielding:

$$\begin{aligned} 0 = &-w f(\sigma,w) + (d-1) w \Gamma(w) - (1-w^2) \Gamma'(w) \\ &+ \frac{\sigma}{v_0 \tau} \left(\int_{-1}^{1} \frac{\mathrm{d}w'}{2W_{d-2}} \left(1-w'^2\right)^{\frac{d-3}{2}} \Gamma(w') - \Gamma(w) \right) . \end{aligned} \tag{10}$$

The flux of particles with radial self-propulsion w arriving at the obstacle's surface from the bulk is proportional to $w f(\sigma, w)$ and is accounted for in the first term of equation (10). A non-zero flux from the bulk implies a non-vanishing surface distribution function $\Gamma(w)$, as seen in equation (10). It is clear from equation (7) that $f(\sigma, w)$ cannot be zero for all w because such a boundary condition would imply a vanishing bulk distribution for all $r > \sigma$. Thus, in the hard-sphere limit, the probability distribution function develops a singular part at contact in the form of a delta peak at $r = \sigma$.

To summarize, denoting $z = r/\sigma$, the stationary distribution function takes the following form:

$$P(\boldsymbol{r}, \boldsymbol{u}) = f(z,w) + \Gamma(w) \delta(z-1) . \tag{11}$$

We have obtained two coupled integro-differential equations satisfied by $f(z,w)$ and $\Gamma(w)$. They depend on a single dimensionless parameter $\eta = \frac{\sigma}{\ell_p}$ comparing the obstacle size to the persistence length $\ell_p = v_0 \tau$. First, the bulk distribution function satisfies for $z > 1$:

$$w \partial_z f + \frac{1-w^2}{z} \partial_w f + \eta f = \eta \rho(z) , \tag{12}$$

with

$$\rho(z) = \int_{-1}^{1} \frac{\mathrm{d}w}{2W_{d-2}} (1-w^2)^{\frac{d-3}{2}} f(z,w) , \tag{13}$$

the bulk density. Second, the surface distribution function follows from:

$$\Gamma'(w) - \frac{w}{1-w^2}(d-1)\Gamma(w) + \frac{\eta}{1-w^2}\Gamma(w) = -\frac{w}{1-w^2} f(1,w) + \frac{\eta}{1-w^2}\hat{\Gamma} , \tag{14}$$

J. Stat. Mech. (2023) 093202

with

$$\hat{\Gamma} = \int_{-1}^{1} \frac{\mathrm{d}w}{2W_{d-2}} (1-w^2)^{\frac{d-3}{2}} \Gamma(w)\,, \tag{15}$$

the surface density. We finally show that the flux balance equation at the obstacle's surface in equation (14) implicitly contains a boundary condition for the bulk distribution function. We can indeed show that $\Gamma(w>0)=0$, which expresses the fact that particles whose self-propulsion points away from the obstacle do not accumulate at its surface. Hence, equation (14) thus yields the boundary condition:

$$f(1,w>0) = \frac{\eta\hat{\Gamma}}{w}\,. \tag{16}$$

As mentioned before, the flux of particles going from the obstacle's surface to the bulk with orientation $w>0$ is proportional to $wf(1,w)$. Equation (16) demonstrates that this flux is independent of the orientation w. This is expected because this flux is uniquely generated by isotropic tumbling events. Indeed, in the absence of tumbling, the particle leaves the obstacle only when $w=0$, see figure 1.

To show that indeed $\Gamma(w>0)=0$, we start by regularizing the product $P(r,w)V'(r)$ in the hard-sphere limit. For this, we integrate once more equation (9) over $r\in[r^*,r']$, thus yielding:

$$\begin{aligned} 0 = &-v_0 w \int_{r^*}^{r'} \mathrm{d}r\, r^{d-1} P(r,w) + \int_{r^*}^{r'} \mathrm{d}r\, r^{d-1} P(r,w) V'(r) \\ &+ \int_{r^*}^{r'} \mathrm{d}r \int_{r^*}^{r} \mathrm{d}r''\, r''^{d-2} \Bigg[v_0(d-1) w P(r'',w) - v_0(1-w^2)\partial_w P(r'',w) \\ &+ \frac{r}{\tau} \left(\int_{-1}^{1} \frac{\mathrm{d}w'}{2W_{d-2}} \left(1-w'^2\right)^{\frac{d-3}{2}} P(r'',w') - P(r'',w) \right) \Bigg]. \end{aligned} \tag{17}$$

We then take the $\epsilon\to 0^+$ limit at fixed r' and afterward, we take the $r'\to\sigma$ limit. The double integral term vanishes, and we are left with

$$\lim_{r'\to\sigma}\lim_{\epsilon\to 0^+} \int_{r^*}^{r'} \mathrm{d}r P(r,w) V'(r) = v_0 w \lim_{r\to\sigma}\lim_{\epsilon\to 0^+} \int_{r^*}^{r'} \mathrm{d}r P(r,w) = v_0 \sigma w \Gamma(w) \tag{18}$$

proving that $\Gamma(w>0)=0$ as $V'(r)<0$ for all r.

3. An integral equation over the density field

In the hard-sphere limit, we have derived the two coupled equations satisfied by the bulk and the surface distribution functions $f(z,w)$ and $\Gamma(w)$, respectively. In this section, we take advantage of the fact that equation (12) satisfied by $f(z,w)$ is

J. Stat. Mech. (2023) 093202

first order in the partial derivatives ∂_z and ∂_w and use the methods of characteristics to recast it into an integral equation for only the spatial density field $\rho(z)$. We furthermore prove that the bulk distribution function $f(z,w)$ exhibits a delta-peak accumulation along typical trajectories of the stochastic dynamics, that we characterize.

The characteristics of equation (12) are parametric lines $(z(s),w(s))$ such that for any function $g(z,w)$ we have:

$$\frac{\mathrm{d}g\left(z(s),w(s)\right)}{\mathrm{d}s} = w(s)\partial_z g\left(z(s),w(s)\right) + \frac{1-w(s)^2}{z(s)}\partial_w g\left(z(s),w(s)\right) . \tag{19}$$

They obey:

$$\begin{cases} z'(s) = w(s)\,, \\ w'(s) = \frac{1-w^2(s)}{z(s)}\,, \end{cases} \tag{20}$$

and are thus lines such that $z\sqrt{1-w^2} = b = \mathrm{cst}$ with b the impact parameter (as indicated in figure 1). They correspond to purely ballistic trajectories and are parametrically depicted in figure 2 as the fictitious time s is increased. Equation (12) is furthermore supplemented with the following boundary condition:

$$f(L, w<0) = 1\,, \tag{21}$$

that implements a homogeneous reservoir of incoming particles at distance L from the obstacle, and where L is sent to infinity at the end of the calculation. As $L\to\infty$, the actual form of the boundary condition at $z=L$ is irrelevant.

We now analyze the behavior of the bulk distribution $f(z,w)$ by dividing the (w,z) plane into four domains, as explained in figure 2.

3.1. Domain 1: $w>0$ and $z\sqrt{1-w^2}<1$

By definition, along a characteristic, the bulk equation reads:

$$f'(s) + \eta f(s) = \eta K(s) \text{ with } K(s) = \rho(z(s))\,, \tag{22}$$

and hence it can be integrated into:

$$f(s,b) = f(s=0,b)\mathrm{e}^{-\eta s} + \eta \mathrm{e}^{-\eta s}\int_0^s \mathrm{d}s' K(s')\mathrm{e}^{\eta s'}\,. \tag{23}$$

A boundary condition must then be implemented to express $f(s=0,b)$ and the (s,b) variables that parametrize the characteristic must be replaced by their (z,w) counterparts. We first solve the equation on the domain $w>0$ and $z\sqrt{1-w^2}<1$. This domain is generated by characteristics corresponding to trajectories leaving the obstacle after a collision. These are depicted in green in figure 2. Along each characteristic, we have:

J. Stat. Mech. (2023) 093202

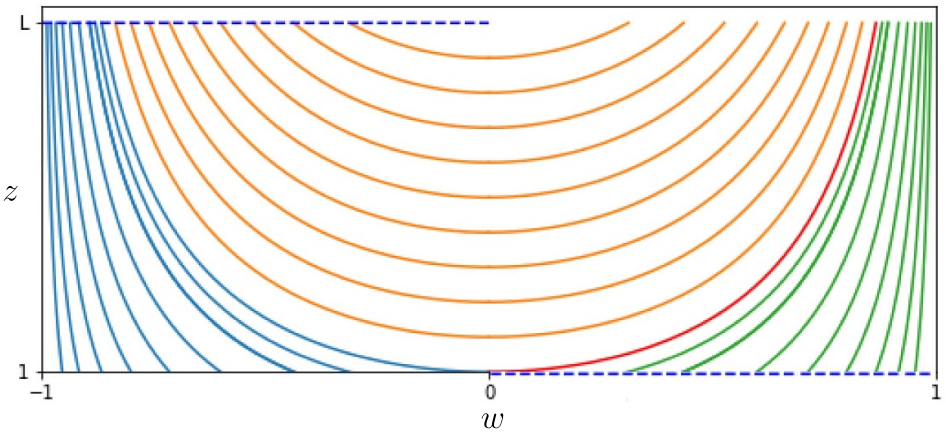

Figure 2. Parametric representation of the characteristics of equation (12) satisfied by the bulk distribution function. The dashed blue lines correspond to the regions of the plane where boundary conditions are specified, see equations (16) and (21). We group the characteristics depending on which boundary condition they intersect and on whether or not they intersect the line $z=1$ representing the obstacle's surface. (Green) Characteristics that are connected to the boundary condition at $z=1$. They correspond to domain 1 of the main text. (Blue) Characteristics that are connected to the boundary condition at radial position $z=L$ and intersect the line at $z=1$. (Orange) Characteristics that are connected to the boundary condition at radial position $z=L$ and do not intersect the line at $z=1$. In the main text, domain 2 comprises all the characteristics restricted to $w<0$ (both blue and orange) and domain 3 comprises the orange characteristics restricted to $w>0$. (Red) The only characteristic that originates from $(z=1, w=0)$ restricted to $w>0$. After each collision, the particle leaves the obstacle exactly along this line (except when it has flipped in course of skidding), see figure 1. We demonstrate that the bulk distribution function develops a singularity along this line which correspond to domain 4 of the main text.

$$z\sqrt{1-w^2} = b < 1\,,$$
$$\Rightarrow\ w(s) = \sqrt{1-\frac{b^2}{z(s)^2}}\,. \tag{24}$$

Thus:

$$z'(s) = \sqrt{1-\frac{b^2}{z(s)^2}}\,,$$
$$\Rightarrow\ z(s)\sqrt{1-\frac{b^2}{z(s)^2}} = s + \sqrt{1-b^2}\,, \tag{25}$$

as we choose to parametrize the characteristics such that $z(s=0)=1$. This leads to:

$$\begin{cases} z(s,b) = \sqrt{s^2 + 2s\sqrt{1-b^2}+1}\,, \\ w(s,b) = \frac{s+\sqrt{1-b^2}}{s^2+2s\sqrt{1-b^2}+1}\,, \end{cases} \tag{26}$$

which can be inverted so as to get:

$$\begin{cases} b = z\sqrt{1-w^2}\,, \\ s = zw - \sqrt{1-z^2(1-w^2)}\,. \end{cases} \tag{27}$$

Finally, from equations (16) and (26), the boundary condition becomes:

$$f(s=0,b) = \frac{\eta\hat{\Gamma}}{\sqrt{1-b^2}}\,. \tag{28}$$

This finally leads to:

$$\begin{aligned} f(z,w) = &\frac{\eta\hat{\Gamma}}{\sqrt{1-z^2(1-w^2)}}\mathrm{e}^{-\eta(zw-\sqrt{1-z^2(1-w^2)})} \\ &+\eta\mathrm{e}^{-\eta zw}\int_1^z \mathrm{d}z'\rho(z')\frac{z'}{\sqrt{z'^2-z^2(1-w^2)}}\mathrm{e}^{\eta\sqrt{z'^2-z^2(1-w^2)}}\,. \end{aligned} \tag{29}$$

3.2. Domain 2: $w<0$

This domain is generated by all characteristics that are connected to the boundary condition at $z=L$ restricted to $w<0$. These are depicted in blue and orange in figure 2. Following the same route as above, we obtain along a characteristic:

$$\begin{cases} z(s,b) = \sqrt{b^2 + \left(s - L\sqrt{1-\frac{b^2}{L^2}}\right)^2}\,, \\ w(s,b) = \frac{-L\sqrt{1-\frac{b^2}{L^2}}+s}{\sqrt{b^2+(s-L\sqrt{1-\frac{b^2}{L^2}})^2}}\,, \end{cases} \tag{30}$$

with $z(s=0,b)=L$. These equations can be inverted to yield:

$$\begin{cases} b = z\sqrt{1-w^2}\,, \\ s = zw + L\sqrt{1-\frac{z^2(1-w^2)}{L^2}}\,. \end{cases} \tag{31}$$

Hence,

J. Stat. Mech. (2023) 093202

$$f(z,w) = \eta \mathrm{e}^{-\eta z w} \int_z^L \mathrm{d}z' \rho(z') \exp\left\{-\eta z' \sqrt{1-\frac{z^2(1-w^2)}{z'^2}}\right\} \frac{1}{\sqrt{1-\frac{z^2(1-w^2)}{z'^2}}} + \mathrm{e}^{-\eta\left(zw+L\sqrt{1-\frac{z^2(1-w^2)}{L^2}}\right)}, = \eta \mathrm{e}^{-\eta z w} \int_z^{+\infty} \mathrm{d}z' \rho(z') \exp\left\{-\eta \sqrt{z'^2 - z^2(1-w^2)}\right\} \frac{z'}{\sqrt{z'^2 - z^2(1-w^2)}}. \tag{32}$$

As expected, the above equation shows the irrelevance of the boundary condition at $z = L$ as L is sent to infinity.

3.3. Domain 3: $w > 0$ and $z\sqrt{1-w^2} > 1$

This domain is generated by the continuation of the orange characteristics of figure 2 analyzed in the previous paragraph into the $w > 0$ half-plane. In this region of the plane, we use the continuity requirement at $w = 0$ inferred from equation (32) as an initial condition at $s = 0$. The characteristics are parametrized by:

$$\begin{cases} w(s,b) = \frac{s}{\sqrt{b^2+s^2}}, \\ z(s,b) = \sqrt{b^2+s^2}, \end{cases} \tag{33}$$

as $w(s=0,b) = 0$. These equations can be inverted to yield:

$$\begin{cases} b = z\sqrt{1-w^2}, \\ s = zw. \end{cases} \tag{34}$$

Furthermore, continuity imposes that:

$$f(s=0,b) = \eta \int_b^{+\infty} \mathrm{d}z' \rho(z') \exp\left\{-\eta z' \sqrt{1-\frac{b^2}{z'^2}}\right\} \frac{1}{\sqrt{1-\frac{b^2}{z'^2}}}, \tag{35}$$

and hence

$$f(z,w) = \eta \mathrm{e}^{-\eta z w} \int_{z\sqrt{1-w^2}}^{+\infty} \mathrm{d}z' \rho(z') \exp\left\{-\eta \sqrt{z'^2 - z^2(1-w^2)}\right\} \frac{z'}{\sqrt{z'^2 - z^2(1-w^2)}} + \eta \mathrm{e}^{-\eta z w} \int_{z\sqrt{1-w^2}}^{z} \mathrm{d}z' \rho(z') \exp\left\{\eta \sqrt{z'^2 - z^2(1-w^2)}\right\} \frac{z'}{\sqrt{z'^2 - z^2(1-w^2)}}. \tag{36}$$

3.4. Domain 4: $w > 0$ and $z\sqrt{1-w^2} = 1$

The line defined by $z\sqrt{1-w^2} = 1$ with $w > 0$, which is depicted in red in figure 2, plays a special role. Indeed, after each collision, the particle leaves the obstacle exactly along this line (except when it has flipped in the course of skidding) and it further keeps traveling along it until its self-propulsion tumbles. This outcome strongly suggests that the bulk

J. Stat. Mech. (2023) 093202

distribution function $f(z,w)$ displays a delta-peak contribution along this characteristic line. To check this, we write:

$$f(z,w) = f_0(z,w) + \phi(z)\delta(z\sqrt{1-w^2}-1)\Theta(w)\,, \tag{37}$$

with $f_0(z,w)$ a piece-wise continuous function (as f_0 might not be continuous while crossing the characteristic line $z\sqrt{1-w^2}=1$ at $w>0$). By inserting the above expression in equation (12), we get, for $z>1$,

$$\left[\sqrt{1-\frac{1}{z^2}}\phi'(z)+\eta\phi(z)\right]\delta(z\sqrt{1-w^2}-1)+w\partial_z f_0+\frac{1-w^2}{z}\partial_w f_0+\eta(f_0-\rho)=0\,, \tag{38}$$

which, in particular, yields:

$$\phi(z) = \phi(1)\mathrm{e}^{-\eta\sqrt{z^2-1}}\,. \tag{39}$$

This shows that the existence of a singularity is equivalent to a non-vanishing $\phi(1)$. Remarkably, the value of $\phi(1)$ can be obtained from the flux-balance equation at the obstacle's surface, equation (14). By integrating it between $w=0^-$ and $w=0^+$ and using $\Gamma(w>0)=0$, we indeed obtain:

$$\Gamma(0^-) = \lim_{\epsilon\to 0}\int_{-\epsilon}^{+\epsilon} \mathrm{d}w\; w f(1,w)\,. \tag{40}$$

Hence,

$$f(1,w) = \frac{\Gamma(0^-)}{w}\delta(w)+\cdots = \Gamma(0^-)\delta(\sqrt{1-w^2}-1)+\cdots\,, \tag{41}$$

where the $\cdots$ stands for something more regular than $\delta(w)/w$. We therefore get $\phi(1)=\Gamma(0^-)$ and thus

$$\phi(z) = \Gamma(0^-)\mathrm{e}^{-\eta\sqrt{z^2-1}}\,. \tag{42}$$

We note that $\Gamma(0^-)$ is proportional to the rate of particles entering the red characteristics of figure 2 from the obstacle and its presence in equation (42) is therefore expected. The existence of a Dirac delta singularity in the distribution function, not only at the surface of the obstacle but also in the bulk of the (w,z) plane, is a remarkable feature of this problem that, as far as we are aware, has not been pointed out in the literature. We believe that this accumulation effect, which a soft-potential would smoothen out, is a generic feature of RTPs around convex rigid obstacles. We furthermore expect that a continuous diffusive motion of the self-propulsion force (instead of a Poisson process as considered here), as is the case in other models of self-propelled particles, such as ABPs [10] and active Ornstein–Uhlenbeck ones [29], would lead to a broadening of this singularity.

J. Stat. Mech. (2023) 093202

3.5. The self-consistency condition

The bulk density $\rho(z)$ satisfies an integral equation that we obtain from equation (13) by integrating equations (29)–(32)–(36)–(42) over the angular variable w. It takes the form of a linear integral equation involving a nonlocal kernel $\mathcal{L}$

$$\rho(z) = \rho_0(z) + \eta \mathcal{L}[\rho](z)\,, \tag{43}$$

where

$$\rho_0(z) = \eta\hat{\Gamma}\int_{\frac{\sqrt{z^2-1}}{z}}^1 \frac{\mathrm{d}w}{2W_{d-2}}(1-w^2)^{\frac{d-3}{2}}\frac{\exp\left\{-\eta\left(zw-\sqrt{1-z^2(1-w^2)}\right)\right\}}{\sqrt{1-z^2(1-w^2)}} + \frac{\Gamma(0^-)}{2W_{d-2}}\frac{\mathrm{e}^{-\eta\sqrt{z^2-1}}}{\sqrt{z^2-1}}z^{2-d}\,, \tag{44}$$

and where the linear operator $\mathcal{L}$ is split into three nonlocal kernels

$$\mathcal{L}[\rho](z) = \mathcal{L}_1[\rho](z) + \mathcal{L}_2[\rho](z) + \mathcal{L}_3[\rho](z)\,, \tag{45}$$

with

$$\mathcal{L}_1[\rho](z) = \int_1^z \mathrm{d}z' z'\rho(z')\int_{\frac{\sqrt{z^2-1}}{z}}^1 \frac{\mathrm{d}w}{2W_{d-2}}(1-w^2)^{\frac{d-3}{2}}\frac{\mathrm{e}^{-\eta z w}\exp\left(\eta\sqrt{z'^2-z^2(1-w^2)}\right)}{\sqrt{z'^2-z^2(1-w^2)}}\,, \tag{46}$$

and

$$\mathcal{L}_2[\rho](z) = 2\int_1^z \mathrm{d}z' z'\rho(z')\int_{\frac{\sqrt{z^2-z'^2}}{z}}^{\frac{\sqrt{z^2-1}}{z}} \frac{\mathrm{d}w}{2W_{d-2}}\left(1-w^2\right)^{\frac{d-3}{2}}\frac{\mathrm{e}^{-\eta z w}\cosh\left(\eta\sqrt{z'^2-z^2(1-w^2)}\right)}{\sqrt{z'^2-z^2(1-w^2)}}\,, \tag{47}$$

and finally

$$\mathcal{L}_3[\rho](z) = \int_z^{+\infty} \mathrm{d}z' z'\rho(z')\int_{-1}^{\frac{\sqrt{z^2-1}}{z}} \frac{\mathrm{d}w}{2W_{d-2}}\left(1-w^2\right)^{\frac{d-3}{2}}\frac{\mathrm{e}^{-\eta z w}\exp\left(-\eta\sqrt{z'^2-z^2(1-w^2)}\right)}{\sqrt{z'^2-z^2(1-w^2)}}\,. \tag{48}$$

To the best of our knowledge, equation (43) can in general only be solved formally:

$$\rho(z) = \sum_{n=0}^{+\infty}\eta^n\mathcal{L}^n[\rho_0](z)\,. \tag{49}$$

Progress can nevertheless be made in some limiting cases. The first one that we study is the near obstacle regime $z-1 \ll 1$ (equivalently $r-\sigma \ll \sigma$) at fixed $\eta = \sigma/\ell_p$. We then determine $\rho(z)$ in the highly ballistic limit $\eta \ll 1$ where the size of the obstacle is much smaller than the persistence length of the self-propelled particle and in a regime such that $\eta z \ll 1$ (equivalently $r \ll \ell_p$). Another case of interest are the corrections to the $\eta \to \infty$ equilibrium limit in which the persistence length is much smaller than the obstacle's size. The first $1/\eta$ correction is equivalent to the case of a single particle against a hard

J. Stat. Mech. (2023) 093202

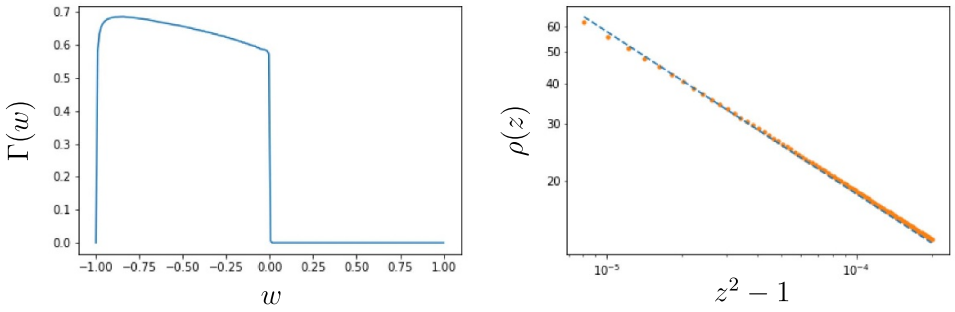

Figure 3. Steady-state distribution of equation (1) for the hard sphere case at $\eta = 1$ in dimension $d = 2$. (Left) Numerically measured surface distribution $\Gamma(w)$. It is non-vanishing for $w < 0$ only and yields $\Gamma(0^-) \simeq 0.57$. (Right) Log–log plot of the bulk space density $\rho(z)$ as a function of $z^2 - 1$ in the vicinity of the obstacle. The dashed blue line is the theoretical prediction of equation (53) with $2W_0 = \pi$ and using the measured value of $\Gamma(0^-)$ from the left panel. The orange dots correspond to numerical simulations. Parameters: $v = 1$, $\tau = 1$, $\sigma = 1$, $L = 100$, $T = 10^{10}$ with T the total physical time.

wall, which was studied (in a two-dimensional geometry) in an earlier study [12]. In that study, the authors notably proved the existence of a delta-peak accumulation at the surface of the wall whose amplitude ($\hat{\Gamma}$ in our language) is proportional to η^{-1}. The situation is, however, very different from the generic η result because in this limit, particles have to tumble to leave the surface of the obstacle. In our language, this corresponds to $\Gamma(0^-) = 0$ (an equality that breaks down at finite values of η, see the numerical results in figure 3) and thus to the absence of a singularity in the bulk of the distribution function. In the ballistic regime, we prove, in section 5, that both $\Gamma(0^-)$ and $\hat{\Gamma}$ have a finite non-zero limit that depends only on the dimension d.

4. Behavior close to the obstacle: activity-induced attraction

In this section, we show that the bulk density $\rho(z)$ diverges close to the obstacle and relate exactly its diverging part to the properties of the surface distribution function $\Gamma(w)$. In the following, we denote $h = z - 1$ and assume that $h \ll 1$. We recall the integral equation in equation (43) satisfied by the bulk density:

$$\rho(z) = \rho_0(z) + \eta \mathcal{L}[\rho](z)\,, \tag{50}$$

with the linear operator $\mathcal{L}$ given in equations (45)–(48). As a first step, we investigate the small distance properties of the function $\rho_0(z)$. We find:

$$\rho_0(1+h) = \frac{\Gamma(0^-)}{2W_{d-2}} \frac{1}{\sqrt{2h}} - \frac{\eta \hat{\Gamma}}{4W_{d-2}} \ln h + O(1)\,. \tag{51}$$

J. Stat. Mech. (2023) 093202

Indeed, the integral term of equation (44) reads in the small h limit:

$$\begin{aligned}\eta\hat{\Gamma}\int_{\frac{\sqrt{z^2-1}}{z}}^{1}\frac{\mathrm{d}w}{2W_{d-2}}(1-w^2)^{\frac{d-3}{2}}\frac{\exp\left\{-\eta\left(zw-\sqrt{1-z^2(1-w^2)}\right)\right\}}{\sqrt{1-z^2(1-w^2)}}\\ =\frac{\eta\hat{\Gamma}}{4W_{d-2}z^{d-2}}\int_0^1\mathrm{d}s\,(1-s)^{\frac{d-3}{2}}\frac{\exp\left(\eta\left(\sqrt{s}-\sqrt{z^2-1+s}\right)\right)}{\sqrt{s}\sqrt{z^2-1+s}},\\ =-\frac{\eta\hat{\Gamma}}{4W_{d-2}}\ln h+O(1).\end{aligned}\tag{52}$$

We find that equation (51) gives the leading order behavior of the actual density field, that is:

$$\rho(1+h)=\frac{\Gamma(0^-)}{2W_{d-2}}\frac{1}{\sqrt{2h}}-\frac{\eta\hat{\Gamma}}{4W_{d-2}}\ln h+O(1).\tag{53}$$

Remarkably, the structure of the near-field density identified in equation (53) is independent of the dimension d for $d\geqslant 2$. It connects (without any free parameters) the divergences of the bulk distribution function on the obstacle to properties of the surface distribution function. We have simulated the dynamics equation (1) in dimension $d=2$ and numerically measured $\Gamma(w)$ and $\rho(z)$. The simulation is performed in a spherical box of radius $L=100v_0\tau$. The boundary condition is such that when the particle hits the outer boundary it is reflected with a random (inward) orientation. In figure 3, we plot the function $\Gamma(w)$ at $\eta=1$ and infer the corresponding value of $\Gamma(0^-)$ from it. We then show that the measured $\rho(z)$ indeed exhibits the square-root divergence predicted by equation (53).

To show the validity of equation (53), our argument goes as follows. We first prove that $\mathcal{L}[\tilde{\rho}](1)$ is finite for any function $\tilde{\rho}(z)$ such that $\tilde{\rho}(1+h)\ln(h)$ is integrable at $h=0$. We then prove that $\rho(1+h)\ln(h)$ is integrable at $h=0$. This result finally implies equation (53) from equation (50). We study the operators $\mathcal{L}_{1,2,3}$ separately. We start by noting that upon a change of variables, we have:

$$\mathcal{L}_1[\tilde{\rho}](1+h)=\frac{(1+h)h}{4W_{d-2}}\int_0^1\mathrm{d}u\,(1+uh)\,\tilde{\rho}\,(1+uh)\,g_1\,(1+uh,1+h)\,,\tag{54}$$

with

$$g_1(z',z)=\int_0^1\mathrm{d}s\frac{(1-s)^{\frac{d-3}{2}}}{\sqrt{z^2-1+s}}\frac{\exp\left(-\eta\sqrt{z^2-1+s}+\eta\sqrt{z'^2-1+z^2s}\right)}{z^2\sqrt{z'^2-1+s}}.\tag{55}$$

For $h\ll 1$, we obtain:

$$\begin{aligned}g_1\,(1+uh,1+h)&\simeq\int_0^1\mathrm{d}s\frac{1}{\sqrt{s\,(s+2h(1+u))}},\\ &\simeq-\ln h\,.\end{aligned}\tag{56}$$

J. Stat. Mech. (2023) 093202

Therefore,

$$\mathcal{L}_1[\tilde{\rho}](1+h) \simeq -\frac{1}{4W_{d-2}} h \ln h \int_0^1 \mathrm{d}u\, \tilde{\rho}(1+uh) \underset{h\to 0}{\to} 0\,, \tag{57}$$

as the function $\tilde{\rho}(1+h)$ is assumed to be integrable at $h=0$. We will proceed accordingly for $\mathcal{L}_2$. We have,

$$\mathcal{L}_2[\tilde{\rho}](1+h) = 2h \int_0^1 \mathrm{d}u\, (1+uh)\, \tilde{\rho}(1+uh)\, g_2\,(1+uh, 1+h)\,, \tag{58}$$

with

$$g_2(z', z) = \int_{\frac{\sqrt{z^2-z'^2}}{z}}^{\frac{\sqrt{z^2-1}}{z}} \frac{\mathrm{d}w}{2W_{d-2}} \left(1-w^2\right)^{\frac{d-3}{2}} \frac{\exp\left(-\eta z w\right)}{\sqrt{z'^2 - z^2(1-w^2)}} \cosh\left(\eta \sqrt{z'^2 - z^2(1-w^2)}\right). \tag{59}$$

For $h \ll 1$, we obtain

$$g_2\,(1+uh, 1+h) \simeq \int_{\sqrt{2h(1-u)}}^{\sqrt{2h}} \frac{\mathrm{d}w}{2W_{d-2}} \frac{1}{\sqrt{2h(u-1)+w^2}}\,, \tag{60}$$

$$\simeq \operatorname{arctanh}\left(\sqrt{u}\right). \tag{61}$$

Hence we get,

$$\mathcal{L}_2[\tilde{\rho}](1+h) \simeq 2h \int_0^1 \mathrm{d}u\, \tilde{\rho}(1+uh) \operatorname{arctanh}\left(\sqrt{u}\right) \underset{h\to 0}{\to} 0\,, \tag{62}$$

by integrability of $\tilde{\rho}$. Finally, we show that if $\tilde{\rho}(1+h)\ln(h)$ is integrable at $h=0$, then $\mathcal{L}_3[\tilde{\rho}](1)$ is finite. From equation (48), the latter yields a finite result if

$$\tilde{\rho}(z') \int_{-1}^{0} \frac{\mathrm{d}w}{2W_{d-2}} \left(1-w^2\right)^{\frac{d-3}{2}} \frac{\exp\left(\eta w - \eta\sqrt{z'^2 - 1 + w^2}\right)}{\sqrt{z'^2 - 1 + w^2}}\,, \tag{63}$$

is integrable at $z'=1$. Furthermore, for $h' = \sqrt{z'^2-1} \ll 1$, we have:

$$\int_{-1}^{0} \frac{\mathrm{d}w}{2W_{d-2}} \left(1-w^2\right)^{\frac{d-3}{2}} \frac{\exp\left(\eta w - \eta\sqrt{z'^2 - 1 + w^2}\right)}{\sqrt{z'^2 - 1 + w^2}} \simeq \frac{-1}{4W_{d-2}} \ln h'\,. \tag{64}$$

Therefore, $\mathcal{L}_3[\tilde{\rho}](1)$ is indeed finite if $\tilde{\rho}\,(1+h)\ln(h)$ is integrable at $h=0$.

Then, if $\rho\,(1+h)\ln(h)$ is integrable, $\mathcal{L}[\rho](1)$ is finite, and we recover equation (53) from equation (50). We now assume that $\rho\,(1+h)\ln(h)$ is not integrable at $h=0$ only to prove that it is not possible at the end. If that is the case, we must have close to $h=0$

$$\rho(1+h) \sim \mathcal{L}[\rho](1+h)\,, \tag{65}$$

J. Stat. Mech. (2023) 093202

since $\rho_0(1+h)\ln(h)$ is integrable at $h=0$. By virtue of equations (57)–(62) and (63)–(64), (65) becomes

$$\rho(1+h) \sim \mathcal{L}_3[\rho](1+h) \sim \int_h \mathrm{d}h' \rho(1+h') \ln(h') \,. \tag{66}$$

However, as we show in appendix B, because $\rho(1+h)$ is integrable at $h=0$, the integral term in the right-hand side of equation (66) grows at most as $\ln h$ close to $h=0$, thus contradicting the initial assumption that $\rho(1+h)\ln(h)$ is not integrable at $h=0$. Therefore, $\rho(1+h)\ln(h)$ is integrable at $h=0$ which in turns implies equation (53).

5. Going highly ballistic

5.1. Steady-state distribution at $\eta = 0$

We now study the solution of equation (43) in the highly ballistic limit $\eta = \sigma/\ell_p \to 0$ and we begin by stating our results. When $\eta = 0$, the surface distribution function is uniform over $w \in [-1,0]$:

$$\Gamma(w) = \frac{1}{d-1}\Theta(-w) \,, \tag{67}$$

and the amplitude of the delta-peak accumulation therefore reads:

$$\hat{\Gamma} = \frac{1}{2(d-1)} \,. \tag{68}$$

Furthermore, for any z fixed (hence for $r \ll \ell_p$), the particle density is given by:

$$\rho(z) = \Theta(z-1)\left[\frac{1}{2} + \frac{\sqrt{z^2-1}}{2W_{d-2}z}\,{}_2F_1\left(\frac{1}{2}, \frac{3-d}{2}, \frac{3}{2}; 1-\frac{1}{z^2}\right) + \frac{1}{2W_{d-2}(d-1)}\frac{z^{2-d}}{\sqrt{z^2-1}}\right] + \frac{1}{2(d-1)}\delta(z-1) \,, \tag{69}$$

where we recall that the boundary conditions are such that $\rho(\infty) = 1$. We introduce the density offset created by the obstacle defined by $K(z) = \rho(z) - 1$. Away from the obstacle, we find a power-law decay:

$$K(z) \sim \frac{1}{2W_{d-2}(d^2-1)}\frac{1}{z^{d+1}} \,, \tag{70}$$

which holds as long as $\eta z \ll 1$ (equivalently $r \ll \ell_p$) after which the density modulations are exponentially suppressed. Importantly, the above expression is integrable at $z \to \infty$ for any $d \geqslant 2$. From there, we obtain the stationary distribution in the (z,w) plane. In domain 1 defined by $w > 0$ and $z\sqrt{1-w^2} < 1$, equation (29) reduces to

$$f(z,w) = 0 \tag{71}$$

J. Stat. Mech. (2023) 093202

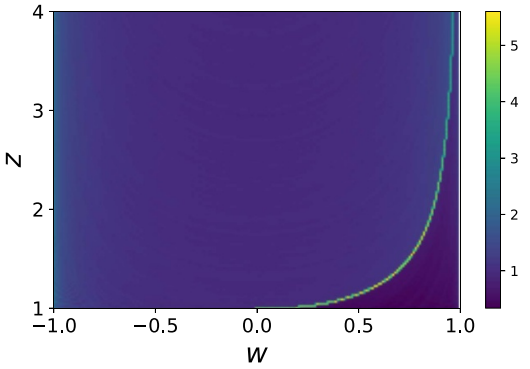

Figure 4. Heatmap of the bulk distribution function $f(z,w)$. It shows two regions of nearly homogeneous densities, one at higher density for $w<0$ and $w>0$ with $z\sqrt{1-w^2}\geqslant 1$ and one at lower density for $w>0$ with $z\sqrt{1-w^2}<1$. The two domains are separated by a line of high density. Parameters: $v=1$, $\tau=1$, $L=10$, $\eta=0.1$ and $T=10^7$ with T the total physical time.

as $\eta\to 0$. In domain 2 defined by $w<0$, equation (32) is given in this limit by:

$$f(z,w)=1+\eta \mathrm{e}^{-\eta z w}\int_z^{+\infty}\mathrm{d}z' K(z')\exp\left\{-\eta\sqrt{z'^2-z^2(1-w^2)}\right\}\frac{z'}{\sqrt{z'^2-z^2(1-w^2)}}, \quad (72)$$

$$=1\,. \quad (73)$$

Finally, in domain 3 defined by $w>0$, and $z\sqrt{1-w^2}>1$ we obtain accordingly from equation (36):

$$f(z,w)=1\,. \quad (74)$$

Therefore, the full bulk distribution reads:

$$f(z,w)=\Theta(-w)+\Theta(w)\left[\Theta(z\sqrt{1-w^2}-1)+\frac{1}{d-1}\delta(z\sqrt{1-w^2}-1)\right]. \quad (75)$$

Figure 4 shows a heatmap of the bulk distribution function $f(z,w)$ at $\eta=0.1$. It exhibits two regions of nearly homogeneous densities, one at higher density for $w<0$ and $w>0$ with $z\sqrt{1-w^2}\geqslant 1$ and one at lower density for $w>0$ with $z\sqrt{1-w^2}<1$. The two domains are separated by a line of high density located at the locus of the delta-peak singularity of equation (75).

We now prove equations (67)–(69) and then we give the expressions of the next-to-leading order $O(\eta)$ corrections to the amplitude of the delta peak showing that the latter is a decreasing function of η. Tumbling thus reduces the fraction of time spent in contact with the obstacle. It follows from equation (43) that, for $z>1$, $K(z)$ is a solution of the integral equation

$$K(z)=K_0(z)+\eta\mathcal{L}[K](z)\,, \quad (76)$$

J. Stat. Mech. (2023) 093202

with $\mathcal{L}$ defined in equations (45)–(48) and where

$$K_0(z) = \rho_0(z) - \int_{\frac{\sqrt{z^2-1}}{z}}^1 \frac{\mathrm{d}w}{2W_{d-2}} \left(1-w^2\right)^{\frac{d-3}{2}} \exp\left(-\eta z w + \eta\sqrt{1-z^2(1-w^2)}\right). \tag{77}$$

So far, $\rho_0(z)$, which is defined in equation (44), explicitly depends on $\Gamma(0^-)$ and $\hat{\Gamma}$. To obtain equation (67) and a closed equation for $K(z)$, we start by defining $K_{\eta=0}(z) = \lim_{\eta\to 0} K(z)$ and, consistently with equation (70), we assume that $K_{\eta=0}(z)$ is integrable as $z\to\infty$. Under this assumption, in the $\eta\to 0$ limit, equation (32) can thus be rewritten as follows:

$$\begin{aligned} f(1, w<0) &= 1 + \eta \mathrm{e}^{-\eta w} \int_1^{+\infty} \mathrm{d}z' \exp\left\{-\eta\sqrt{z'^2-(1-w^2)}\right\} \frac{K(z')z'}{\sqrt{z'^2-(1-w^2)}}, \\ &= 1 + \eta \int_1^{+\infty} \mathrm{d}z' \frac{K_{\eta=0}(z')z'}{\sqrt{z'^2-(1-w^2)}} + o(\eta). \end{aligned} \tag{78}$$

Together with equation (14), the above equation therefore yields equation (67):

$$\Gamma(w) = \frac{1}{d-1}\Theta(-w) + \eta\Gamma_1(w) + o(\eta), \tag{79}$$

where the correcting term $\Gamma_1(w)$ is, for $w<0$, a solution of:

$$\Gamma_1'(w) - \frac{w}{1-w^2}(d-1)\Gamma_1(w) = -\frac{w}{1-w^2}\int_1^{+\infty} \mathrm{d}z' \frac{K_{\eta=0}(z')z'}{\sqrt{z'^2-(1-w^2)}} - \frac{1}{2(d-1)(1-w^2)}. \tag{80}$$

We defer to section 5.2 the study of the small η corrections, but we note that equation (67) follows from equation (79) obtained under the sole assumption that $K_{\eta=0}(z)$ is integrable as $z\to\infty$. To leading order in η, we thus obtain from equation (77):

$$\lim_{\eta\to 0} K_0(z) = \left[-\frac{1}{2} + \frac{\sqrt{z^2-1}}{2W_{d-2}r}\,{}_2F_1\left(\frac{1}{2}, \frac{3-d}{2}, \frac{3}{2}; 1-\frac{1}{z^2}\right) + \frac{1}{2W_{d-2}(d-1)}\frac{z^{2-d}}{\sqrt{z^2-1}}\right], \tag{81}$$

which is integrable for $z\to\infty$. The rest of the proof follows from the fact that if $K_{\eta=0}(z)$ is integrable at $z\to\infty$ then $\lim_{\eta\to 0}\mathcal{L}[K](z)$ exists. We first notice that:

$$\lim_{\eta\to 0}\mathcal{L}_1[K](z) = \int_1^z \mathrm{d}z'\, z'\, K_{\eta=0}(z') \int_{\frac{\sqrt{z^2-1}}{z}}^1 \frac{\mathrm{d}w}{2W_{d-2}} \frac{\left(1-w^2\right)^{\frac{d-3}{2}}}{\sqrt{z'^2 - z^2\left(1-w^2\right)}}. \tag{82}$$

The above integral is indeed well-defined as:

$$\int_{\frac{z^2-1}{z}}^1 \frac{\mathrm{d}w}{2W_{d-2}} \frac{\left(1-w^2\right)^{\frac{d-3}{2}}}{\sqrt{z'^2 - z^2\left(1-w^2\right)}}, \tag{83}$$

J. Stat. Mech. (2023) 093202

remains finite at $z'=1$ and $K_{\eta=0}(z')$ is integrable at $z'=1$. Accordingly, the same holds for $\mathcal{L}_2$ since

$$\lim_{\eta\to 0}\mathcal{L}_2[K](z)=2\int_1^z \mathrm{d}z' z' K_{\eta=0}(z')\int_{\frac{\sqrt{z^2-z'^2}}{z}}^{\frac{\sqrt{z^2-1}}{z}}\frac{\mathrm{d}w}{2W_{d-2}}\frac{\left(1-w^2\right)^{\frac{d-3}{2}}}{\sqrt{z'^2-z^2(1-w^2)}}. \tag{84}$$

We now turn to the study of $\mathcal{L}_3$. We recall equation (48):

$$\mathcal{L}_3[K](z)=\int_z^{+\infty}\mathrm{d}z' z' K(z')\int_{-1}^{\frac{\sqrt{z^2-1}}{z}}\frac{\mathrm{d}w}{2W_{d-2}}\left(1-w^2\right)^{\frac{d-3}{2}}\times \tag{85}$$

$$\cdots\times\frac{\exp\left(-\eta z w-\eta\sqrt{z'^2-z^2(1-w^2)}\right)}{\sqrt{z'^2-z^2(1-w^2)}}, \tag{86}$$

from which it appears that if $K_{\eta=0}(z')$ is integrable at $+\infty$, then

$$\lim_{\eta\to 0}\mathcal{L}_3[K](z)\ \text{exists.} \tag{87}$$

The integrability of $\lim_{\eta\to 0}K_0(z)$ for $z\to\infty$ therefore guarantees that for $z>1$

$$K(z)=K_0(z)+\eta\lim_{\eta\to 0}\mathcal{L}[K_0](z)+o(\eta), \tag{88}$$

which self-consistently proves the integrability of $K_{\eta=0}(z)$ which is our starting assumption. Equation (69) then follows immediately. The result in equation (69) is independent of the persistence length ℓ_p of the RTP. It only depends on σ through the rescaling $r=\sigma z$.

Two interesting results follow. First, the main results of this section, notably equations (67)–(69)–(75), also hold for different classes of self-propelled particles [10, 29]. For ABPs whose self-propulsion has norm v_0 and correlation time τ, the steady-state distribution function also depends only on z and w and obeys:

$$0=-\left(w\partial_r P(z,w)+\frac{1-w^2}{z}\partial_w P(z,w)\right)+\frac{1}{z^{d-1}}\partial_z\left(z^{d-1}P(z,w)\partial_z V(z)\right)+\eta\mathcal{R}P(z,w), \tag{89}$$

with $\mathcal{R}$ an operator independent of η accounting for the reorientation of the active self-propulsion, for example, an earlier study [10] presents a comparative review of run-and-tumble and ABPs. In the limit $\eta\to 0$, the subtleties associated to the details of the operator $\mathcal{R}$ are therefore suppressed, and our results derived for RTPs are expected to hold. We also conjecture that our results also hold for active Ornstein–Uhlenbeck particles [29], which may come as more of a surprise since the norm of the active self-propulsion fluctuates in this model. Here, the steady-state distribution function indeed depends on (z,w) and on v the self-propulsion velocity. We denote $v_0=\langle v\rangle$ its average and introduce as before $\eta=\sigma/(v_0\tau)$. The steady-state distribution obeys:

J. Stat. Mech. (2023) 093202

$$0 = -\left(w\partial_r P(z,w,v) + \frac{1-w^2}{z}\partial_w P(z,w,v)\right) + \frac{1}{z^{d-1}}\partial_z\left(z^{d-1}P(z,w,v)\frac{v_0}{v}\partial_z V(z)\right) + \frac{v_0}{v}\eta\mathcal{R}P(z,w,v) \tag{90}$$

with $\mathcal{R}$ another operator independent of η accounting for the reorientation of the active self-propulsion. In the $\eta \to 0$ limit, and in the hard-sphere limit where the prefactor $\frac{v_0}{v}$ in front of the gradient of the potential becomes irrelevant, it follows that v and (z,w) decouple in the steady-state and that the results obtained in this section for RTPs provide the correct marginal in the (z,w) space of the steady-state distribution of a highly ballistic active Ornstein–Uhlenbeck particle interacting with a hard-sphere obstacle.

Finally, equation (69) also corresponds to the steady-state distribution function of two highly ballistic RTPs interacting via hard-core repulsion—or equivalently the low-density pair-distribution function of a fluid of highly ballistic hard-core RTPs—with σ representing the diameter of a single particle. Indeed, the relative separation $\boldsymbol{r} = \boldsymbol{r}_1 - \boldsymbol{r}_2$ of the two RTPs, with self-propulsions along $\boldsymbol{u}_1$ and $\boldsymbol{u}_2$, evolves according to:

$$\frac{\mathrm{d}\boldsymbol{r}}{\mathrm{d}t} = v_0||\boldsymbol{u}_1 - \boldsymbol{u}_2||\boldsymbol{n} - 2\boldsymbol{\nabla}V(\boldsymbol{r})\,, \tag{91}$$

with the relative self-propulsion direction:

$$\boldsymbol{n} = \frac{\boldsymbol{u}_1 - \boldsymbol{u}_2}{||\boldsymbol{u}_1 - \boldsymbol{u}_2||}\,, \tag{92}$$

At large distances, $\boldsymbol{n}$ is isotropically distributed on the unit sphere. Therefore, in the highly ballistic limit, where the self-propulsion $\boldsymbol{n}$ is only set by boundary conditions, the problem maps to that of a single RTP studied in this work. With the highly ballistic steady-state distribution function being independent of the persistence length ℓ_p, equation (69) also holds for a pair of highly ballistic particles.

5.2. Corrections to the ballistic limit

Equation (80) gives the first-order corrections to the ballistic limit of the surface term of the steady-state distribution function. Imposing integrability at $w = -1$, we obtain in dimension $d = 2$,

$$\Gamma_1(w) = \frac{-(2+\pi w)\sqrt{1-w^2} + \pi\left(-\pi + \arccos(w)\right) - 2w^2\mathrm{arctanh}(\sqrt{1-w^2})}{4\pi\sqrt{1-w^2}}\,, \tag{93}$$

thus yielding

$$\hat{\Gamma} = \frac{1}{2} - \eta\frac{4C-2+\pi}{8\pi} + o(\eta)\,, \tag{94}$$

with $C \simeq 0.92$ Catalan's constant. We numerically confirm the decay of the amplitude of the surface term predicted by equation (94) as shown in figure 5. In dimension $d = 3$, equation (80) allows to express $\Gamma_1(w)$ in terms of K and E, which are the complete elliptic integrals of the first and second kinds, respectively:

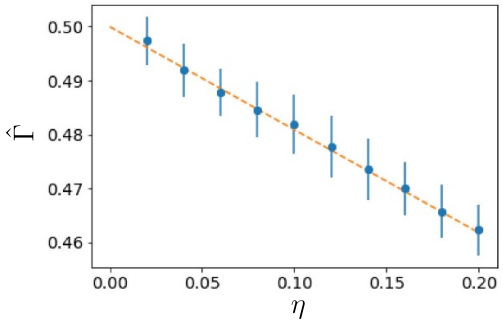

Figure 5. Amplitude of the delta-peak accumulation at the surface of the obstacle $\hat{\Gamma}$ in dimension $d=2$ as a function of the ratio η of the obstacle size over the persistence length of the RTP. The dashed orange line is the theoretical prediction of equation (94). The blue dots correspond to numerical simulations at fixed persistence length with varying obstacle sizes. Parameters: $v=1$, $\tau=1$, $L=20$, $T=10^{10}$ with T the total physical time.

$$\Gamma_1(w)=\frac{6w^2K\left(1-w^2\right)+3\pi\left(w^2-1\right)w\,{}_2F_1\left(-\frac{1}{2},\frac{3}{2};2;1-\frac{1}{w^2}\right)-4w^3-6E\left(1-w^2\right)+6w+2}{24\left(w^2-1\right)}. \tag{95}$$

We therefore obtain

$$\hat{\Gamma}=\frac{1}{4}-c\eta+o(\eta)\,, \tag{96}$$

with the constant c given by

$$c=-\int_{-1}^{0}\frac{\mathrm{d}w}{2}\Gamma_1(w)\simeq 0.053\,. \tag{97}$$

6. The effect of hydrodynamic interactions

In the above, we studied the steady-state distribution function of an RTP around a fixed spherical obstacle. In the highly ballistic limit, the latter matches the steady-state distribution of two RTPs with hard-core repulsion. In the present section, we consider the motion of two RTPs interacting via hydrodynamic interactions carried by a Stokesian fluid of viscosity μ and a repulsive hardcore potential in dimension $d\geqslant 3$. We deal with colloids driven by an external force and endowed with a no-slip boundary condition at their surface, as can be implemented by trapping them in mobile optical traps [30]. In the overdamped limit, the equations of motion express a balance between the propulsion force, the potential interaction between the particles, and the force exerted by the surrounding fluid on each of them. This results in an effective position-dependent mobility for each particle, given to leading order in their relative

J. Stat. Mech. (2023) 093202

separation by the Oseen tensor. The Oseen tensor is the first term of an infinite series in powers of σ/r, which does not fully capture near-field phenomenology by overestimating the mobility in that regime [31]. Retaining the Oseen tensor only, as we shall now implement, can be seen as a first step toward understanding the role of hydrodynamics. As in the dry case, we find that in this approximation the steady-state distribution displays a singular-at-contact delta-peak accumulation. Furthermore, we show that the main features of the highly ballistic bulk density obtained in the previous section, that are a square root divergence close to the contact and a power-law decay with exponent -4 in $d=3$ at large distances (but on scales smaller than the persistence length) survive. The latter feature, the r^{-4} decay, is likely to be robust upon expanding beyond the Oseen approximation. Our study also predicts a reduced sticking coefficient compared to the dry case. Refined results on the effect of hydrodynamic interactions can be obtained by using the Rotne–Prager–Yamakawa [32, 33] approximation and subsequent expansions of the mobility tensor as derived by Felderhof [34]. For completeness, we provide in appendix C a derivation of the equations of motion used in this section. Upon explicitly reintroducing a mobility ω for the purpose of the discussion, these can be written as follows:

$$\begin{cases} 0 = f_0\boldsymbol{u}_1 - \boldsymbol{\nabla}_{\boldsymbol{r}}V(\boldsymbol{r}) - \omega\left[\frac{\mathrm{d}\boldsymbol{r}_1}{\mathrm{d}t} - A(r)\frac{\mathrm{d}\boldsymbol{r}_2}{\mathrm{d}t} - (d-2)A(r)\frac{1}{r^2}\left(\boldsymbol{r}\cdot\frac{\mathrm{d}\boldsymbol{r}_2}{\mathrm{d}t}\right)\boldsymbol{r}\right], \\ 0 = f_0\boldsymbol{u}_2 + \boldsymbol{\nabla}_{\boldsymbol{r}}V(\boldsymbol{r}) - \omega\left[\frac{\mathrm{d}\boldsymbol{r}_2}{\mathrm{d}t} - A(r)\frac{\mathrm{d}\boldsymbol{r}_1}{\mathrm{d}t} - (d-2)A(r)\frac{1}{r^2}\left(\boldsymbol{r}\cdot\frac{\mathrm{d}\boldsymbol{r}_1}{\mathrm{d}t}\right)\boldsymbol{r}\right], \end{cases} \tag{98}$$

with $\boldsymbol{r}=\boldsymbol{r}_1-\boldsymbol{r}_2$ and

$$\omega = \mu\frac{d(d-2)}{d-1}\frac{\Omega_d\sigma^{d-2}}{2^{d-2}},$$

$$A(r) = \frac{d}{2(d-1)}\left(\frac{\sigma}{2r}\right)^{d-2}, \tag{99}$$

yielding

$$\left[1 + A(r) + (d-2)\frac{A(r)}{r^2}(\boldsymbol{r}\cdot)\boldsymbol{r}\right]\frac{\mathrm{d}\boldsymbol{r}}{\mathrm{d}t} = \frac{f_0}{\omega}(\boldsymbol{u}_1-\boldsymbol{u}_2) - \frac{2}{\omega}\boldsymbol{\nabla}_{\boldsymbol{r}}V(\boldsymbol{r}). \tag{100}$$

To first order in $r \gg \sigma$, we can easily invert this equation and obtain

$$\frac{\mathrm{d}r^\alpha}{\mathrm{d}t} = M^{\alpha\beta}\left(v_0\left(u_1^\beta - u_2^\beta\right) - 2\partial_\beta V(r)\right), \tag{101}$$

with $v_0 = f_0/\omega$ and where we have rescaled the potential $V(\boldsymbol{r}) \to V(\boldsymbol{r})/\omega$. The tensor $M^{\alpha\beta}$ is given by

$$M^{\alpha\beta} = \delta^{\alpha\beta}(1-A(r)) - (d-2)A(r)\frac{r^\alpha r^\beta}{r^2}, \tag{102}$$

which allows us rewrite the equation of motion as:

J. Stat. Mech. (2023) 093202

$$\frac{\mathrm{d}\boldsymbol{r}}{\mathrm{d}t} = (1-A(r))\,v_0\,(\boldsymbol{u}_1-\boldsymbol{u}_2) - v_0(d-2)A(r)\,[(\boldsymbol{u}_1-\boldsymbol{u}_2)\cdot\hat{\boldsymbol{r}}]\,\hat{\boldsymbol{r}} - 2\,(1-(d-1)A(r))\,\boldsymbol{\nabla}_{\boldsymbol{r}}V(\boldsymbol{r})\,. \tag{103}$$

Several comments are in order. First, the amplitude of the pairwise forces is reduced due to hydrodynamic interactions. Second, the effective propulsion velocity is also reduced and it becomes space dependent: the velocity is lower as the particles get closer. Third, there is also an extra force along $\hat{\boldsymbol{r}}$. Note that it is repulsive if $(\boldsymbol{u}_1-\boldsymbol{u}_2)\cdot\hat{\boldsymbol{r}}<0$ and attractive if $(\boldsymbol{u}_1-\boldsymbol{u}_2)\cdot\hat{\boldsymbol{r}}>0$. We show that this results in a reduced delta-peak attraction with respect to the dry case. The stationary state distribution function $g_0(\boldsymbol{r};\boldsymbol{u}_1,\boldsymbol{u}_2)$ is the solution of:

$$0 = -\partial_\alpha\left(g_0 M^{\alpha\beta}\left(v_0\left(\boldsymbol{u}_1^\beta-\boldsymbol{u}_2^\beta\right)-2\partial^\beta V(\boldsymbol{r})\right)\right)+\mathcal{R}g_0\,, \tag{104}$$

where the operator $\mathcal{R}$, which is negligible in the highly ballistic limit, accounts for the reorientation of the active forces. In this limit, when the pair-potential is taken to be of the hard-sphere type, the bulk distribution function f obeys:

$$w\,[1-(d-1)A(z)]\,\partial_z f + (1-A(z))\,\frac{1-w^2}{z}\partial_w f = 0\,. \tag{105}$$

with w the cosine of the angle between $\boldsymbol{u}_1-\boldsymbol{u}_2$ and $\hat{\boldsymbol{r}}$ and $z=r/\sigma$. Furthermore, the surface term satisfies:

$$\Gamma'(w)-(d-1)\frac{w}{1-w^2}\Gamma(w) = -f(\sigma,w)\frac{w}{1-w^2}\left[1-\frac{(d-2)A(\sigma)}{1-A(\sigma)}\right], \tag{106}$$

$$= -(d-1)f(1,w)\frac{w}{1-w^2}\left(\frac{1-d2^{1-d}}{d-1-d2^{1-d}}\right). \tag{107}$$

for $w<0$ and $\Gamma(w>0)=0$. In the highly ballistic limit, the bulk distribution function f is constant along the characteristics of equation (105), which read:

$$z\sqrt{1-w^2}\left[1-\frac{d}{2}\left(\frac{1}{2z}\right)^{d-2}\right]^{\frac{1}{d-1}} = b\,, \tag{108}$$

with b the far away impact parameter. In $d=3$, this leads to:

$$f(z,w) = \Theta(-w)+\Theta(w)\left[\Theta\left(\sqrt{(1-w^2)z(4z-3)}-1\right)+\frac{1}{2}\delta\left(\sqrt{(1-w^2)z(4z-3)}-1\right)\right]. \tag{109}$$

Accordingly, the density can be obtained for $z>1$ as:

$$\rho(z) = \frac{1}{2}+\frac{1}{2}\sqrt{\frac{z(4z-3)-1}{z(4z-3)}}+\frac{1}{4\sqrt{z(4z-3)}}\frac{1}{\sqrt{z(4z-3)-1}}\,. \tag{110}$$

J. Stat. Mech. (2023) 093202

This shows that the square-root divergence of the bulk density close to $z = 1$ identified in section 4 is robust to the inclusion of far-field hydrodynamic interactions, though it remains an open question to find out how near-field corrections would affect this behavior. The far-field structure of the density field is also left unchanged by hydrodynamic interactions as we obtain $\rho(z) \sim z^{-4}$ for $z \gg 1$, similarly to the $d = 3$ case of equation (69). Finally, the surface term can be deduced for $w < 0$ from equation (106) as follows:

$$\begin{aligned}\Gamma(w) &= \frac{1 - d2^{1-d}}{d - 1 - d2^{1-d}}, \\ &= \frac{1}{d-1} + \frac{d2^{1-d}(2-d)}{(d-1)(d-1-d2^{1-d})} < \frac{1}{d-1}.\end{aligned} \tag{111}$$

The amplitude of the sticking term is therefore reduced by far-field hydrodynamic interactions (from 1/2 without hydrodynamic interactions down to 1/5 when they are included, in $d = 3$).

7. Conclusion

We have analytically studied the steady state of an RTP around a hard spherical obstacle. We have shown that as soon as the self-propulsion force has a non-vanishing correlation time, the RTP is effectively attracted to the obstacle when in its vicinity. This effect manifests in two ways. First, the steady-state distribution function displays a delta-peak accumulation at the obstacle's surface. Second, the bulk density diverges with an exponent $-1/2$ close to it because the radial velocity of a particle leaving the obstacle vanishes provided that it does not flip its orientation in the course of skidding. We then obtained the full steady-state distribution function in the limit where the persistence length of the RTP is much larger than the obstacle size. This also gives us the pair-distribution function at low density for a fluid of highly ballistic hard-core RTPs. We furthermore showed that the amplitude of the delta-peak accumulation is an increasing function of the persistence length, at least when the latter is still large compared to the obstacle size. Finally, we have investigated the role of far-field hydrodynamic interactions on colloids driven by an external force, as captured by the Oseen tensor. Importantly, we conjecture that hydrodynamic interactions reduce the propensity of highly persistent RTPs to stick together while preserving the qualitative features of the bulk density. It would certainly be interesting to investigate the robustness of the structure of the distribution function not only upon incorporating near-field hydrodynamic effects but also by considering different propulsion mechanisms in the spirit of [35]. Other stimulating open questions are concerned with non-spherical obstacles for which the far-field decay of the density field is known to be drastically different [36]. The separation of the steady-state probability distribution into a bulk distribution and a surface distribution is expected to survive.

J. Stat. Mech. (2023) 093202

Appendix A. Dynamics in the r, w variables

The dynamics in equation (1) is closed in terms of the variables r and w. We discuss the resulting dynamics for the case of a hard spherical obstacle. In between two tumbles, say at t_0 and t_1, and while the particle is away from the obstacle $r(t) \geqslant \sigma$, we have:

$$r(t) = \sqrt{r(t_0)^2 + v_0^2 (t-t_0)^2 + 2v_0 (t-t_0) r(t_0) w(t_0)}\,, \tag{A.1}$$

together with

$$w(t) = \frac{v_0 (t-t_0) + w(t_0) r(t_0)}{r(t)}\,. \tag{A.2}$$

The last two equations are obtained by projecting equation (1) along $\boldsymbol{r}$ and $\boldsymbol{u}$. Let us now assume that the particle hits the obstacle at some intermediate time t_2 such that $r(t_2) = \sigma$. For all $t_2 \leqslant t \leqslant t_1$ such that $w(t) < 0$, the particle skids on the obstacle and

$$r(t) = \sigma\,, \tag{A.3}$$

while

$$w(t) = \frac{e^{\frac{2v_0(t-t_0)}{\sigma}} (1 + w(t_2)) + w(t_2) - 1}{e^{\frac{2v_0(t-t_0)}{\sigma}} (1 + w(t_2)) + 1 - w(t_2)}\,. \tag{A.4}$$

Finally, when a tumble occur, the new value of w is sampled with the measure $P_{\text{tumble}}(w) = (2W_{d-2})^{-1} \left(1 - w^2\right)^{\frac{d-3}{2}}$. With increasing the dimension, $P_{\text{tumble}}(w)$ gets more biased towards $w = 0$, the counterpart of the increasing number of directions orthogonal to $\boldsymbol{r}$.

Appendix B. Bound on the growth in equation (66)

In this appendix, we show that if $\rho(z)$ is an integrable function at $z = 1$, the integral in equation (66):

$$I = \int_h^a \mathrm{d}h' \rho(1 + h') \ln(h')\,, \tag{B.1}$$

does not grow faster than $\ln h$ as $h \to 0$ for any finite $a > 0$. Let

$$P(h) = \int_0^h \rho(1 + h') \mathrm{d}h'\,. \tag{B.2}$$

It is such that $P(h) \to 0$ as $h \to 0$. By integration by part we have:

$$I = P(a) \ln a - P(h) \ln h - \int_h^a \frac{P(h')}{h'}\,. \tag{B.3}$$

J. Stat. Mech. (2023) 093202

We can finally write:

$$\int_h^a \frac{P(h')}{h'} < P(a)\,(\ln a - \ln h)\,, \tag{B.4}$$

that proves that I does not grow faster than $\ln h$ as $h \to 0$.

Appendix C. Derivation of the equations of motion with hydrodynamic interactions

C.1. Fluid flow around a moving obstacle

We consider a moving spherical obstacle of radius $\sigma/2$ at velocity $\boldsymbol{u}$. The fluid is incompressible and viscous with viscosity μ and the flow is given by the Stokes equation with no-slip boundary conditions:

$$\begin{cases} \mu\Delta\boldsymbol{v} - \boldsymbol{\nabla}P = 0\,, \\ \boldsymbol{\nabla}\cdot\boldsymbol{v} = 0\,, \\ \boldsymbol{v}(\boldsymbol{r} = (\sigma/2)\hat{\boldsymbol{r}}) = \boldsymbol{u}\,, \\ P(\boldsymbol{r}) = P_\infty \text{ as } ||\boldsymbol{r}|| \to \infty\,. \end{cases} \tag{C.1}$$

We hereafter follow another study [37]. Due to the linearity of the equations in $\boldsymbol{u}$, we introduce M^α_β and X_β such that

$$\begin{cases} v^\alpha(\boldsymbol{r}) = M^\alpha_\beta(\boldsymbol{r})\boldsymbol{u}^\beta\,, \\ P(\boldsymbol{r}) - P_\infty = \eta X_\beta(\boldsymbol{r})\boldsymbol{u}^\beta\,. \end{cases} \tag{C.2}$$

They satisfy:

$$\begin{cases} \partial_\beta\partial^\beta M^\alpha_\gamma - \partial^\alpha X_\gamma = 0\,, \\ \partial_\alpha M^\alpha_\gamma = 0\,, \\ M^\beta_\gamma(\boldsymbol{r} = (\sigma/2)\hat{\boldsymbol{r}}) = \delta^\beta_\gamma\,, \\ X_\beta(\boldsymbol{r}) = 0 \text{ as } ||\boldsymbol{r}|| \to \infty\,, \end{cases} \tag{C.3}$$

which is a completely rotationally invariant set of equations. We have hence by symmetry

$$\begin{cases} X_\beta(\boldsymbol{r}) = f(r)\boldsymbol{r}_\beta\,, \\ M^\alpha_\gamma(\boldsymbol{r}) = M_1(r)\delta^\alpha_\gamma + M_2(r)\boldsymbol{r}^\alpha\boldsymbol{r}_\gamma\,. \end{cases} \tag{C.4}$$

We can therefore obtain a set of three coupled equations for f, M_1 and M_2 as follows:

$$\begin{cases} M_1'' + \frac{d-1}{r}M_1' + 2M_2 - f = 0\,,\ M_1(\sigma/2) = 1\,, \\ M_2'' + \frac{d-1}{r}M_2' + \frac{4M_2'}{r} - \frac{f'}{r} = 0\,,\ M_2(\sigma/2) = 0\,, \\ \frac{M_1'}{r} + rM_2' + (d+1)M_2 = 0\,. \end{cases} \tag{C.5}$$

J. Stat. Mech. (2023) 093202

Combining them so as to express the vanishing of the Laplacian of the pressure field, we arrive at:

$$f'' + \frac{d+1}{r} f' = 0\,, \tag{C.6}$$

so that

$$f(r) = \frac{A}{r^d}\,. \tag{C.7}$$

While injecting this expression into the second equation of equation (C.5), we obtain $M_2(r)$ as follows:

$$M_2(r) = \frac{A}{2r^d}\left(1 - \frac{\sigma^2}{4r^2}\right), \tag{C.8}$$

which in turn can eventually be plugged into the first equation of equation (C.5) so as to get:

$$M_1(r) = \frac{A}{2d}\left(\frac{\sigma^2}{4r^d} - \frac{1}{r^{d-2}}\right) + \frac{\sigma^{d-2}}{2^{d-2}r^{d-2}}\,. \tag{C.9}$$

The constant A can then be obtained thanks to the divergenceless condition of the velocity field. This eventually yields the pressure and velocity fields which are given by:

$$\begin{cases} P(\boldsymbol{r}) = P_\infty + \mu \frac{d(d-2)}{d-1} \frac{2}{\sigma} \left(\frac{\sigma}{2r}\right)^{d-1} \hat{\boldsymbol{r}} \cdot \boldsymbol{u}\,, \\ \boldsymbol{v}(\boldsymbol{r}) = \frac{1}{2(d-1)} \left(\frac{\sigma}{2r}\right)^{d} \left[d\left(\frac{2r}{\sigma}\right)^2 + (d-2)\right] \boldsymbol{u} + \frac{d(d-2)}{2(d-1)} \left(\frac{\sigma}{2r}\right)^{d} \left[\left(\frac{2r}{\sigma}\right)^2 - 1\right] (\hat{\boldsymbol{r}} \cdot \boldsymbol{u})\, \hat{\boldsymbol{r}}\,. \end{cases} \tag{C.10}$$

C.2. Two moving spheres and hydrodynamic interactions

We now consider the case of two spheres of radius $\sigma/2$ at positions $\boldsymbol{r}_1$ and $\boldsymbol{r}_2$ with velocities $\boldsymbol{u}_1$ and $\boldsymbol{u}_2$, respectively. The flow field is given by the solution of the Stokes equation subjected to the proper boundary conditions:

$$\begin{cases} \mu \Delta \boldsymbol{v} - \boldsymbol{\nabla} P = 0\,, \\ \boldsymbol{\nabla} \cdot \boldsymbol{v} = 0\,, \\ \boldsymbol{v}(\boldsymbol{r}_1 + (\sigma/2)\hat{\boldsymbol{r}}) = \boldsymbol{u}_1\,, \\ \boldsymbol{v}(\boldsymbol{r}_2 + (\sigma/2)\hat{\boldsymbol{r}}) = \boldsymbol{u}_2\,. \end{cases} \tag{C.11}$$

In this case, we look for the solution as:

$$\begin{cases} \boldsymbol{v}(\boldsymbol{r}) = \boldsymbol{v}_1^{(0)}(\boldsymbol{r} - \boldsymbol{r}_1) + \boldsymbol{v}_2^{(0)}(\boldsymbol{r} - \boldsymbol{r}_2) + \boldsymbol{v}_{corr}(\boldsymbol{r})\,, \\ P(\boldsymbol{r}) = P_0^{(0)}(\boldsymbol{r} - \boldsymbol{r}_1) + P_0^{(0)}(\boldsymbol{r} - \boldsymbol{r}_2) + P_{corr}(\boldsymbol{r}) + P_\infty\,, \end{cases} \tag{C.12}$$

J. Stat. Mech. (2023) 093202

with $\boldsymbol{v}_1^{(0)}(\boldsymbol{r}-\boldsymbol{r}_1)$ the fluid flow due to particle 1 in absence of particle 2 (and accordingly for particle 2 and for the pressure fields). The correcting terms satisfy the following system of equations:

$$\begin{cases} \mu\Delta\boldsymbol{v}_{\rm corr} - \boldsymbol{\nabla}P_{\rm corr} = 0\,, \\ \boldsymbol{\nabla}\cdot\boldsymbol{v}_{\rm corr} = 0\,, \\ \boldsymbol{v}_{\rm corr}(\boldsymbol{r}_1 + (\sigma/2)\hat{\boldsymbol{r}}) = -\boldsymbol{v}_2^{(0)}(\boldsymbol{r}_1 - \boldsymbol{r}_2 + (\sigma/2)\hat{\boldsymbol{r}})\,, \\ \boldsymbol{v}_{\rm corr}(\boldsymbol{r}_2 + (\sigma/2)\hat{\boldsymbol{r}}) = -\boldsymbol{v}_1^{(0)}(\boldsymbol{r}_2 - \boldsymbol{r}_1 + (\sigma/2)\hat{\boldsymbol{r}})\,. \end{cases} \tag{C.13}$$

The correcting velocity field $\boldsymbol{v}_{\rm corr}$ vanishes as the separation between the two particles goes to infinity (comparatively to their size). In the following, we will be interested in the first correction of $v_{\rm corr}$ in the inverse separation $\sigma/||\boldsymbol{r}_1-\boldsymbol{r}_2||$. We define $\delta\boldsymbol{v}_2 = \boldsymbol{v}_2^{(0)}(\boldsymbol{r}_1-\boldsymbol{r}_2+\sigma/2\hat{\boldsymbol{r}})$, and accordingly $\delta\boldsymbol{v}_1 = \boldsymbol{v}_1^{(0)}(\boldsymbol{r}_2-\boldsymbol{r}_1+\sigma/2\hat{\boldsymbol{r}})$, which, from C.1, writes to leading order in the inverse separation:

$$\delta\boldsymbol{v}_2 = \frac{d(d-2)}{2(d-1)}\left(\frac{\sigma}{2|\boldsymbol{r}_1-\boldsymbol{r}_2|}\right)^{d-2}\frac{((\boldsymbol{r}_1-\boldsymbol{r}_2)\cdot\boldsymbol{u}_2)\,(\boldsymbol{r}_1-\boldsymbol{r}_2)}{|\boldsymbol{r}_1-\boldsymbol{r}_2|^2} \tag{C.14}$$

$$+\frac{d}{2(d-1)}\left(\frac{\sigma}{2|\boldsymbol{r}_1-\boldsymbol{r}_2|}\right)^{d-2}\boldsymbol{u}_2 + O\left(\left(\frac{\sigma}{2|\boldsymbol{r}_1-\boldsymbol{r}_2|}\right)^{d-1}\right), \tag{C.15}$$

which is therefore independent of $\hat{\boldsymbol{r}}$. As a consequence, up to their first-order correction in the inverse separation, the velocity and pressure fields are given by the sum of the fields sourced by two isolated spherical particles with shifted velocities: one at $\boldsymbol{r}_1$ with velocity $\boldsymbol{u}_1-\delta\boldsymbol{v}_2$ and one at $\boldsymbol{r}_2$ with velocity $\boldsymbol{u}_2-\delta\boldsymbol{v}_1$. Hence

$$\begin{aligned} \boldsymbol{v}(\boldsymbol{r}) = {} & \frac{1}{2(d-1)}\left(\frac{\sigma}{2|\boldsymbol{r}-\boldsymbol{r}_1|}\right)^d\left[d\left(\frac{2|\boldsymbol{r}_1-\boldsymbol{r}|}{\sigma}\right)^2+(d-2)\right](\boldsymbol{u}_1-\delta\boldsymbol{v}_2) \\ & + \frac{1}{2(d-1)}\left(\frac{\sigma}{2|\boldsymbol{r}-\boldsymbol{r}_2|}\right)^d\left[d\left(\frac{2|\boldsymbol{r}_2-\boldsymbol{r}|}{\sigma}\right)^2+(d-2)\right](\boldsymbol{u}_2-\delta\boldsymbol{v}_1) \\ & + \frac{d(d-2)}{2(d-1)}\left(\frac{\sigma}{2|\boldsymbol{r}_1-\boldsymbol{r}|}\right)^d\left[\left(\frac{2|\boldsymbol{r}_1-\boldsymbol{r}|}{\sigma}\right)^2-1\right]\frac{((\boldsymbol{r}-\boldsymbol{r}_1)\cdot(\boldsymbol{u}_1-\delta\boldsymbol{v}_2))\,(\boldsymbol{r}-\boldsymbol{r}_1)}{|\boldsymbol{r}-\boldsymbol{r}_1|^2} \\ & + \frac{d(d-2)}{2(d-1)}\left(\frac{\sigma}{2|\boldsymbol{r}_2-\boldsymbol{r}|}\right)^d\left[\left(\frac{2|\boldsymbol{r}_2-\boldsymbol{r}|}{\sigma}\right)^2-1\right]\frac{((\boldsymbol{r}-\boldsymbol{r}_2)\cdot(\boldsymbol{u}_2-\delta\boldsymbol{v}_1))\,(\boldsymbol{r}-\boldsymbol{r}_2)}{|\boldsymbol{r}-\boldsymbol{r}_2|^2}\,. \end{aligned} \tag{C.16}$$

Accordingly, the pressure field is given by:

$$\begin{aligned} P(\boldsymbol{r}) = {} & P_\infty + \mu\frac{d(d-2)}{d-1}\frac{2}{\sigma}\left(\frac{\sigma}{2|\boldsymbol{r}-\boldsymbol{r}_1|}\right)^{d-1}\frac{(\boldsymbol{r}-\boldsymbol{r}_1)\cdot(\boldsymbol{u}_1-\delta\boldsymbol{v}_2)}{|\boldsymbol{r}-\boldsymbol{r}_1|} \\ & + \mu\frac{d(d-2)}{d-1}\frac{2}{\sigma}\left(\frac{\sigma}{2|\boldsymbol{r}-\boldsymbol{r}_2|}\right)^{d-1}\frac{(\boldsymbol{r}-\boldsymbol{r}_2)\cdot(\boldsymbol{u}_2-\delta\boldsymbol{v}_1)}{|\boldsymbol{r}-\boldsymbol{r}_2|}\,. \end{aligned} \tag{C.17}$$

We now seek to compute the force exerted by the fluid flow on particle 1:

$$\boldsymbol{F} = \int \mathrm{d}\mathbb{S} \cdot \boldsymbol{\pi}\,, \tag{C.18}$$

with $\pi_{ij} = -P\delta_{ij} + \eta\left(\partial_i v_j + \partial_j v_i\right)$ the stress tensor. One can check that to next to leading order in the relative separation, the force exerted by the fluid on particle 1 is the same as the one exerted on an isolated particle with velocity $\boldsymbol{u}_1 - \delta\boldsymbol{v}_2$, that is:

$$\boldsymbol{F} = -\mu \frac{d(d-2)}{d-1} \frac{\Omega_d \sigma^{d-2}}{2^{d-2}} (\boldsymbol{u}_1 - \delta\boldsymbol{v}_2)\,. \tag{C.19}$$

The equations of motion (98) of the main text then follow.

References

[1] Vicsek T, Czirók A, Ben-Jacob E, Cohen I and Shochet O 1995 Novel type of phase transition in a system of self-driven particles *Phys. Rev. Lett.* **75** 1226–9

[2] Grégoire G and Chaté H 2004 Onset of collective and cohesive motion *Phys. Rev. Lett.* **92** 025702

[3] Ramaswamy S 2010 The mechanics and statistics of active matter *Annu. Rev. Condens. Matter Phys.* **1** 323–45

[4] Tailleur J and Cates M E 2008 Statistical mechanics of interacting run-and-tumble bacteria *Phys. Rev. Lett.* **100** 218103

[5] Redner G S, Hagan M F and Baskaran A 2013 Structure and dynamics of a phase-separating active colloidal fluid *Phys. Rev. Lett.* **110** 055701

[6] Fily Y and Marchetti M C 2012 Athermal phase separation of self-propelled particles with no alignment *Phys. Rev. Lett.* **108** 235702

[7] Cates M E and Tailleur J 2015 Motility-induced phase separation *Annu. Rev. Condens. Matter Phys.* **6** 219–44

[8] Tailleur J and Cates M E 2009 Sedimentation, trapping and rectification of dilute bacteria *Europhys. Lett.* **86** 60002

[9] Pototsky A and Stark H 2012 Active Brownian particles in two-dimensional traps *Europhys. Lett.* **98** 50004

[10] Solon A P, Cates M E and Tailleur J 2015 Active Brownian particles and run-and-tumble particles: a comparative study *Eur. Phys. J. Spec. Top.* **224** 1231–62

[11] Fodor E, Hayakawa H, Tailleur J and van Wijland F 2018 Non-Gaussian noise without memory in active matter *Phys. Rev.* E **98** 062610

[12] Ezhilan B, Alonso-Matilla R and Saintillan D 2015 On the distribution and swim pressure of run-and-tumble particles in confinement *J. Fluid Mech.* **781** R4

[13] Wagner C G, Hagan M F and Baskaran A 2017 Steady-state distributions of ideal active Brownian particles under confinement and forcing *J. Stat. Mech.* 043203

[14] Fan Lee C 2013 Active particles under confinement: aggregation at the wall and gradient formation inside a channel *New J. Phys.* **15** 055007

[15] Elgeti J and Gompper G 2015 Run-and-tumble dynamics of self-propelled particles in confinement *Europhys. Lett.* **109** 58003

[16] Spagnolie S E, Moreno-Flores G R, Bartolo D and Lauga E 2015 Geometric capture and escape of a microswimmer colliding with an obstacle *Soft Matter* **11** 3396–411

[17] Goldstein H, Poole C and Safko J 1950 *Classical Mechanics* (*AW Series in Advanced Physics*) (Addison-Wesley Press)

[18] Van den Broeck C and Hänggi P 1984 Activation rates for nonlinear stochastic flows driven by non-gaussian noise *Phys. Rev.* A **30** 2730

[19] Schnitzer M J 1993 Theory of continuum random walks and application to chemotaxis *Phys. Rev.* E **48** 2553

[20] Solon A P, Fily Y, Baskaran A, Cates M E, Kafri Y, Kardar M and Tailleur J 2015 Pressure is not a state function for generic active fluids *Nat. Phys.* **11** 673–8

[21] Dhar A, Kundu A, Majumdar S N, Sabhapandit S and Schehr G 2019 Run-and-tumble particle in one-dimensional confining potentials: steady-state, relaxation and first-passage properties *Phys. Rev.* E **99** 032132

J. Stat. Mech. (2023) 093202

[22] Thompson A G, Tailleur J, Cates M E and Blythe R A 2011 Lattice models of nonequilibrium bacterial dynamics *J. Stat. Mech.* P02029
[23] Slowman A B, Evans M R and Blythe R A 2016 Jamming and attraction of interacting run-and-tumble random walkers *Phys. Rev. Lett.* **116** 218101
[24] Malakar K, Jemseena V, Kundu A, Vijay Kumar K, Sabhapandit S, Majumdar S N, Redner S and Dhar A 2018 Steady state, relaxation and first-passage properties of a run-and-tumble particle in one-dimension *J. Stat. Mech.* 043215
[25] Härtel A, Richard D and Speck T 2018 Three-body correlations and conditional forces in suspensions of active hard disks *Phys. Rev.* E **97** 012606
[26] Agoritsas E 2021 Mean-field dynamics of infinite-dimensional particle systems: global shear versus random local forcing *J. Stat. Mech.* 033501
[27] Mo R, Liao Q and Xu N 2020 Rheological similarities between dense self-propelled and sheared particulate systems *Soft Matter* **16** 3642–8
[28] de Pirey T A, Lozano G and van Wijland F 2019 Active hard spheres in infinitely many dimensions *Phys. Rev. Lett.* **123** 260602
[29] Martin D, O'Byrne J, Cates M E, Fodor E, Nardini C, Tailleur J and van Wijland F 2021 Statistical mechanics of active Ornstein-Uhlenbeck particles *Phys. Rev.* E **103** 032607
[30] Berner J, Müller B, Ruben Gomez-Solano J, Krüger M and Bechinger C 2018 Oscillating modes of driven colloids in overdamped systems *Nat. Commun.* **9** 999
[31] Guazzelli E and Morris J F 2011 *A Physical Introduction to Suspension Dynamics* vol 45 (Cambridge University Press)
[32] Rotne J and Prager S 1969 Variational treatment of hydrodynamic interaction in polymers *J. Chem. Phys.* **50** 4831–7
[33] Yamakawa H 1970 Transport properties of polymer chains in dilute solution: hydrodynamic interaction *J. Chem. Phys.* **53** 436–43
[34] Felderhof B U 1977 Hydrodynamic interaction between two spheres *Physica* A **89** 373–84
[35] Matas-Navarro R, Golestanian R, Liverpool T B and Fielding S M 2014 Hydrodynamic suppression of phase separation in active suspensions *Phys. Rev.* E **90** 032304
[36] Granek O, Baek Y, Kafri Y and Solon A P 2020 Bodies in an interacting active fluid: far-field influence of a single body and interaction between two bodies *J. Stat. Mech.* 063211
[37] Brenner H 1981 The translational and rotational motions of an n-dimensional hypersphere through a viscous fluid at small reynolds numbers *J. Fluid Mech.* **111** 197–215

J. Stat. Mech. (2023) 093202